

---

# Depth-Wise Emergence of Prediction-Centric Geometry in Large Language Models

---

Shahar Haim<sup>1</sup> Daniel C. McNamee<sup>1</sup>

## Abstract

We show that decoder-only large language models exhibit a depth-wise transition from context-processing to prediction-forming phases of computation accompanied by a reorganization of representational geometry. Using a unified framework combining geometric analysis with mechanistic intervention, we demonstrate that late-layer representations implement a structured geometric code that enables selective causal control over token prediction. Specifically, angular organization of the representation geometry parametrizes prediction distributional similarity, while representation norms encode context-specific information that does not determine prediction. Together, these results provide a mechanistic-geometric account of the dynamics of transforming context into predictions in LLMs.

## 1. Introduction

Ongoing efforts seek to understand how large language models (LLMs) implement their remarkable predictive capabilities. Two broad approaches have emerged. One line of work focuses on geometric analyses of representational flow through the residual stream, characterizing how token representations evolve across depth using measures such as similarity (Ethayarajh, 2019; Barbero et al., 2024), dimensionality (Cheng et al., 2025; Skean et al., 2025; Sarfati et al., 2024), curvature (Hosseini & Fedorenko, 2023; Skean et al., 2025), and isotropy (Cai et al., 2021; Razzhigaev et al., 2024). This geometric perspective has revealed systematic depth-dependent structure and increasingly abstract representations, but it primarily tracks how contextual input representations are transformed through the network. As a result, it remains largely *context-centric* and descriptive, offering limited insight into which aspects of representational geometry are functionally responsible for determining model predictions.

---

<sup>1</sup>Champalimaud Centre for the Unknown, Lisbon, Portugal.

A complementary line of work adopts a mechanistic, intervention-based perspective, seeking to understand LLM computation by perturbing internal representations and observing changes in predicted output token distributions. These approaches directly target the functional role of internal states in shaping model behavior and have revealed depth-dependent sensitivity to different classes of interventions (Turner et al., 2023; Engels et al., 2025; Yu et al., 2025). However, intervention-based studies typically operate without an explicit representational framework, leaving unclear how the manipulated representations are geometrically organized or which representational degrees of freedom are causally relevant beyond linear separability (Mikolov et al., 2013; Conneau et al., 2018; Saglam et al., 2025). Consequently, while geometric analyses lack causal specificity, mechanistic interventions, though *prediction-centric* often lack a principled account of representational structure.

In this work, we demonstrate that these two perspectives are separately incomplete and must be integrated to yield a mechanistic understanding of LLM computation. Indeed, probe techniques (Alain & Bengio, 2016; Conneau et al., 2018) linking internal representation to functional performance have ultimately proven misleading whereby decoders point to the presence of relevant information that is not causally involved in how the overall network generates output (Ravichander et al., 2021; Hewitt & Liang, 2019; Elazar et al., 2020). Similarly, it has been demonstrated that attention weights in transformers (Jain & Wallace, 2019) and feature maps in deep networks in general (Ribeiro et al., 2016; Adebayo et al., 2018; Lapuschkin et al., 2019) do not specifically highlight the relevant elements of internal representation that contributes to functional performance.

We address this challenge by combining geometric analysis with causal intervention in a focused case study of what we term *mechanistic geometry*: representational geometry whose structure is directly tied to causal control over prediction. Using this integrated approach, we identify a specific geometric schema by which the identity of predicted tokens is encoded in decoder-only LLMs. We show that this schema is causally selective, operates over distinct geometric degrees of freedom, and is localized to late layers following a sharp depth-wise transition from context-processing to prediction-forming computation. This transition marks

not merely a shift in representational content, but a reorganization of representation space into a form that directly supports selective causal control over token prediction.

### 1.1. Related Work and Background

**Latent space geometry in LLMs.** A prominent line of work investigates the internal computation of large language models by analyzing the geometry of latent token representations across depth. These studies characterize sets of token embeddings using a range of geometric and statistical measures in order to describe how representation spaces are reorganized across layers.

The measures employed span different relational orders of geometric structure. At the local level, pairwise measures quantify distances between token representations, including cosine similarity (Ethayarajh, 2019) and distance (Barbero et al., 2024). Higher-order measures include curvature, which characterizes the geometry of token triplets (Hosseini & Fedorenko, 2023; Skean et al., 2025). At the global level, set-level measures quantify the structure of entire collections of representations, including effective or intrinsic dimensionality estimated via variance-based decompositions (Sarfati et al., 2024; Skean et al., 2025; Razzhigaev et al., 2024), neighbor-distance-based estimators (Cheng et al., 2025), and isotropy or embedding dispersion (Cai et al., 2021; Razzhigaev et al., 2024).

Together, these analyses demonstrate that layer-wise geometric organization provides a meaningful description of how representation spaces are transformed across depth. However, this literature is almost exclusively input-centric and does not relate geometric structure to output distributions or prediction behavior.

The linear representation hypothesis formalizes how concepts can be geometrically encoded as directions under an appropriate inner product (Park et al., 2023). Our results refine this picture by showing that, even when such linear structure is present and decodable, only a subset of angular geometry is causally responsible for prediction, and that this structure emerges specifically in late, prediction-forming layers. From this perspective, our findings suggest that the applicability of linear representations may be layer-dependent, with distinct inner products becoming appropriate at different stages of computation, particularly across the transition from context-processing to prediction-forming phases.

#### Depth-dependent representational dynamics in LLMs.

A growing body of work has documented systematic depth-dependent changes in the representations of LLMs, characterized by shifts in dimensionality, geometry, and decodability. Using cross-sequence representational analyses, recent studies have identified a peak in dimensionality in early-to-

mid layers of LLMs, followed by improved linear decodability of high-level semantic information (Saglam et al., 2025; Cheng et al., 2025). Based on dimensionality estimators and probes, these effects have been interpreted as reflecting a high-dimensional abstraction regime. However, these analyses focus exclusively on input representations and do not relate representational geometry to output generation or prediction similarity.

In parallel, work leveraging within-sequence representations (Razzhigaev et al., 2024; Skean et al., 2025) has examined representational dynamics within a single forward pass and reported non-monotonic geometric changes across layers. While these studies point to depth-dependent structure in representational trajectories, they primarily characterize local within-prompt dynamics and do not distinguish between computations supporting contextual processing and those supporting prediction-level behavior.

More directly related, Lad et al., 2025 propose a functional distinction between early input-centric and later prediction-centric computation in LLMs, based on analyses of attention patterns, single-neuron activity, and layerwise ablations. This work provides evidence for a functional transition across depth, but does not examine representational geometry, leaving open how internal representations are reorganized to support prediction-centric computation.

Finally, a retrospective comparison across intervention-based studies reveals a consistent dichotomy that has not previously been articulated. Interventions derived from input representations tend to be most effective in early layers (Turner et al., 2023; Engels et al., 2025), whereas interventions constructed from output derived representations are most effective in later layers (Yu et al., 2025). Despite their complementary empirical profiles, these approaches have not been unified under a common geometric framework or directly related to depth-dependent changes in representational structure. Together, prior work documents depth-dependent representational structure, functional input–output distinctions, and complementary intervention effects, but does not identify distinct regimes of geometric organization or causally connect representational geometry to prediction distributions.

In this work, we provide such a unified geometric and causal account by identifying a sharp transition from input-centric to prediction-centric representations and showing how specific geometric degrees of freedom in late layers causally govern token prediction behavior.

## 2. Methodology

**Models.** Throughout this work we use three widely used open-source decoder-only LLMs. These models represent different architectural families while having comparable

parameter scales: Llama V3.1 8B (Dubey et al., 2024), Mistral 0.3 7B (Jiang et al., 2023), and Qwen 2.5 7B (Qwen et al., 2025). Henceforth we refer to these models as Llama, Mistral, and Qwen.

## 2.1. Intervention setup

**The Months task.** We use the Months task as introduced by Engels et al., 2025: “*Let’s do some calendar math. [INTERVAL] months from [MONTH] is*”, where *INTERVAL* takes values from {One, Two,..., Twelve}, and *MONTH* can be any month of the year. In total, this task has 144 prompts that correspond to every combination of *INTERVAL* and *MONTH*. To simplify, for each prompt we read out only the logits of the 12 month of the year and choose the largest one to be the output. The modular arithmetic design of this task creates a closed input-output space where each prompt maps to a single output, but a single output is appropriate for multiple input prompts. Using the abstracted notation from Engels et al., 2025 we can define an input-output pair as  $\alpha + \beta = \gamma$  where  $\alpha + \beta$  corresponds to the input (starting month and interval), and  $\gamma$  corresponds to the output prediction (target month). In this task the models accuracies are: Llama 95%, Mistral 85% and Qwen 70% .

**Context input-centric intervention.** An *input-centric intervention* attempts to alter the input representation by intervening on the hidden-layer activations of specific input tokens in the context window (for intuition see Fig. S1). In the Months task, this corresponds to shifting the representation from a given input of the form  $\alpha + \beta$  toward some  $\alpha' + \beta$  or  $\alpha + \beta'$ , and by that effectively biasing the model toward a new target prediction  $\gamma'$ .

Here, we calculate steering vectors *per layer* based on centroid differences between tokens of interest. For example, for the tokens corresponding to  $\alpha$  and a target token  $\alpha'$ , we compute the centroid of all hidden-state vectors corresponding to occurrences of  $\alpha$  and  $\alpha'$  in the prompts at a given layer  $L$ . The steering vector from  $\alpha$  to  $\alpha'$  at layer  $L$  is then defined as

$$V_L(\alpha, \alpha') = \mathbb{E}_{t \sim \alpha'}[h_L(t)] - \mathbb{E}_{t \sim \alpha}[h_L(t)],$$

where  $h_L(t)$  denotes the hidden representation of token  $t$  at layer  $L$ . We apply the intervention by simply adding this vector to the hidden representation of the corresponding input token at layer  $L$ . To quantify the effect of such intervention we quantify the change in models prediction preference between the new and old targets:  $(\text{Logit}_{\text{after}}(\gamma') - \text{Logit}_{\text{after}}(\gamma)) - (\text{Logit}_{\text{before}}(\gamma') - \text{Logit}_{\text{before}}(\gamma))$ . If the intervention had no effect we expect a value of zero, and a positive value if the intervention shifted the preference towards the new target.

**Predicted output-centric intervention.** An *output-centric intervention* attempts to directly influence the model’s output prediction by intervening on the hidden-layer activations of the final token, whose representation is used to produce the output. Unlike input-centric interventions, this method steers the model’s output toward a desired target by using representations associated with that outcome (for intuition see Fig. S1). In the Months task, this corresponds to shifting the representation of the last token from one associated with a target prediction  $\gamma$  toward that of a different prediction  $\gamma'$ .

Prediction-centric steering vectors are computed by taking centroid differences between last-token representations of prompts whose model prediction is  $\gamma$  and those whose prediction is  $\gamma'$ . Concretely, for each layer  $L$ , we group prompts according to their *baseline model prediction* and compute the centroids of the hidden representations of the final token for prompts whose prediction is  $\gamma$  and those whose prediction is  $\gamma'$ . The prediction-centric steering vector is then defined as the difference between these centroids. Unlike the input-centric intervention, which isolates specific input properties, this method directly targets prediction-level representations. As in the input-centric case, the intervention is applied via simple vector addition, but here the steering vector is added only to the final token. The effect of this intervention is also quantified by the change in the models prediction preference.

## 2.2. Representation analyses

**Representation analyses data.** To inspect the geometry of LLMs representations across layers, and how they are transformed we use data from the wiki-text-103-raw-v1 dataset (Merity et al., 2017). We collect two sets of sequences: Short context (15 tokens) and long context (500-600 tokens). Each of these sets will be used both as ordered and shuffled sequences. Each set consists of one thousand sequences. We chose our dataset based on length criteria as measured by the original tokenized sequence. For semantic completeness we require all sequences end with the dot at the end of a sentence, thus long contexts have a slightly variable length. We parse the text so that the end of every sequence is “.” to keep the final token identical across sequences. For shuffled sequences, we remove the dot at the end of the sequence, shuffle the words, and add the dot back. Therefore, all used sequences end with an identical token. In the following, when analyzing identical tokens, we refer to the last tokens of each sequence. When analyzing non-identical tokens we refer to tokens that are located fourth from the end. Such tokens are located closely to the last tokens, but naturally vary between sequences.

**Dimensionality analysis.** For a set of tokens in some LLM layer we measure the distribution of variance across or-

thogonal dimensions by using the Participation Ratio (PR):

$$PR = \frac{\left(\sum_{i=1}^d \lambda_i\right)^2}{\sum_{i=1}^d \lambda_i^2}, \lambda_i = \sigma_i^2$$

Where  $\sigma_i$  are the singular values of a matrix. Here, specifically, we decompose matrices who's entries are the hidden layer activations of a set of tokens. Higher PR indicates that variance is distributed across a larger number of orthogonal directions. Due to the sensitivity of variance based decompositions to outliers, we perform the decomposition after normalizing each token vector. The normalized results preserve the same trends in data while attenuating outlier driven distortions. We provide the unnormalized analyses results in the supplementary for comparison (See [Results](#), [Context- and token-dependent dimensionality across layers](#)).

### 3. Results

**Two phases of computation in LLMs.** To explicitly study context-centric and prediction-centric representational dynamics we first seek to implicate representations across LLM layers as causally contributing to either. To do so we intervene on hidden layer activations of three LLMs performing the Months task with two types of interventions: (1) an *input-centric intervention* and (2) an *prediction-centric intervention* (See [Methodology](#), [Interventions](#)). For each prompt, we sweep intervention directions toward all month centroids, using the prompt's input month (input-centric) or the model's predicted month (prediction-centric) as the source. Strikingly, across models, we find that applying a layer-wise *input-centric* intervention to the starting month token has dominant effect during an early phase of the models. This early phase occupies roughly the first two thirds of layers. In stark contrast, applying a layer-wise *prediction-centric* intervention to the last token has a dominant effect during the late phase of the models, occupying roughly the last third of layers. To ensure the observed effects are unrelated to some coupling between the manipulated input tokens and predicted tokens (both being months), we apply the *input-centric* intervention to the interval tokens, instead of the input month tokens. Again, the effect is observable during the early phase of the models (Fig. 1).

The intervention experiments reveal a clear dissociation across depth, with early layers selectively sensitive to input-centric perturbations and later layers selectively sensitive to prediction-centric perturbations. This pattern suggests that early layers perform computations that directly depend on input representations, while later layers perform a computation utilizing transformed representations in a prediction-oriented manner. To examine whether this functional dissociation is reflected in representation geometry, we analyze the dimensional structure of token representations across layers using the Participation Ratio on a more diverse dataset.

### Context- and token-dependent dimensionality across layers.

To isolate the contribution of contextual variability to token representations, we compare the geometric structure of pilot-token representations between *identical* tokens appearing at the end of different sequences and *non-identical* tokens positioned closely in the sequence (see [Methodology](#), [Representation analyses](#)). In this setting, the participation ratio (PR) quantifies the effective dimensionality of representational variability across tokens, capturing how variation induced by context and token identity is distributed across dimensions. To isolate the contribution of contextual variability to token representations, we compare the geometric structure of pilot-token representations between *identical* tokens appearing at the end of different sequences and *non-identical* tokens positioned closely in the sequence (see [Methodology](#), [Representation analyses](#)). In this setting, the PR quantifies the effective dimensionality of representational variability across tokens, capturing how variation induced by context and token identity is distributed across dimensions.

We examine the dimensionality of the subspace occupied by these two token sets under four contextual conditions: long or short sequences that are either ordered or shuffled. These conditions allow us to independently control for context length and contextual coherence. For each condition, token set, and layer, we compute the PR for both unnormalized and normalized token representations. Normalization yields highly similar trends across layers while producing more stable and consistent PR estimates for Mistral. We therefore focus on normalized PR results in the main text and provide unnormalized results in the Supplementary (Fig. S3). To more directly isolate the effect of contextual coherence, we further baseline the PR of ordered sequences by the corresponding shuffled condition, yielding a differential measure that emphasizes coherence-related differences (Fig. 2). For completeness, the original normalized PR curves without baselining are shown in Fig. S2.

A clear contrast emerges between the PR profiles of identical and non-identical tokens. Identical-token representations undergo a context-sensitive expansion followed by contraction of their effective dimensionality in the early layers, after which PR stabilizes with depth. In contrast, non-identical tokens exhibit broader and often multi-peaked PR profiles, reflecting variability driven jointly by token identity and contextual differences distributed across layers. For both token sets, PR is modulated by contextual coherence, with ordered sequences tending to occupy higher-dimensional subspaces than shuffled ones (Fig. 2; see also Figs. S2, S3), suggesting that coherent context induces richer representational variability.

As a control, we measure PR for short, ordered sequences in untrained models (Figs. S2, S3). These exhibit qualitatively

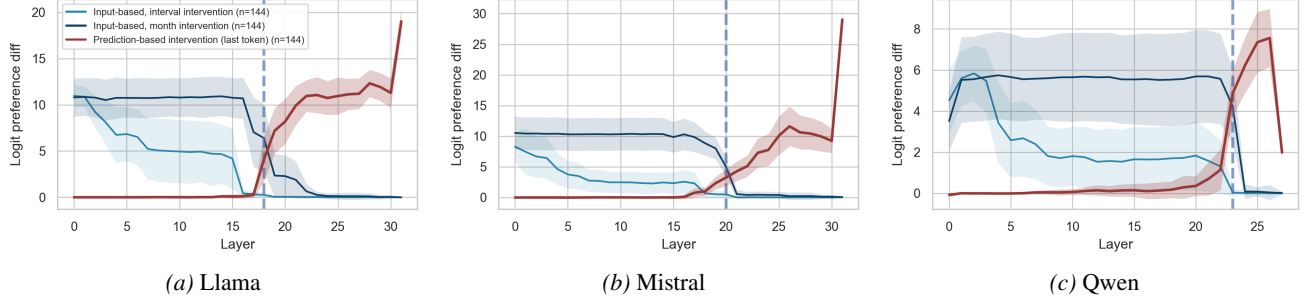


Figure 1. Per-layer intervention experiment results. Average logit preference difference: blue curves for input based interventions (interval and month), Red curve for output based intervention. The blue vertical line marks the phase-change point.

different PR profiles for both identical and non-identical tokens, indicating that the observed patterns are learned properties of trained models rather than architectural artifacts.

Taken together, these results reveal a depth-dependent reorganization of representational geometry consistent with the intervention findings. Early layers exhibit context-sensitive variability, particularly for identical tokens, while later layers exhibit more stable dimensional structure. Alongside the non-identical token results, this points to a geometric organization that depends jointly on context and token identity. We next analyze pairwise Euclidean and angular distances to relate this reorganization to model predictions in a prediction-centric framework.

**Two-component geometric coding in the prediction-centric phase.** Previous analyses identified a context-dependent and token-sensitive spatial reorganization during the first, input-centric computational phase in LLMs. These reorganized representations are propagated to the subsequent, prediction-centric phase. To characterize how this geometry relates to model outputs, we analyze representations with respect to final prediction distributions using the same two sets of pilot tokens introduced above.

For each layer and condition, we compute pairwise Euclidean and angular distances between all token representations within each pilot-token set, and quantify prediction differences by the symmetric KL divergence between the corresponding output distributions. We then compute the layer-wise Spearman correlation between representational distance and prediction divergence.

For identical tokens, both Euclidean and angular distances exhibit gradually increasing positive correlations with prediction divergence across depth (Supp. Fig. S4), indicating that geometric proximity increasingly mirrors prediction similarity as representations propagate. In contrast, for non-identical tokens this correspondence breaks down (Fig. 3). Angular distances in ordered sequences remain uncorrelated with prediction divergence in early layers, but begin

to exhibit a clear positive correlation during the second, prediction-centric phase. This transition aligns with the depth at which prediction-centric interventions become effective, suggesting that first-phase reorganization establishes an angular geometry that becomes predictive of output distributions in the second phase.

By contrast, Euclidean distances for non-identical tokens show no stable relationship with prediction divergence, indicating that Euclidean proximity is largely orthogonal to predictive similarity in this regime. Although Euclidean and angular distances are directly related,  $\|X - Y\|_2^2 = \|X\|_2^2 + \|Y\|_2^2 - 2\|X\|_2\|Y\|_2 \cos(\theta)$ , a divergence between them reflects variability in vector norms. The observed dissociation therefore indicates that, for non-identical tokens, norm fluctuations contribute strongly to Euclidean distances while remaining largely uncoupled from prediction similarity.

This interpretation is consistent with our earlier perturbation results. In that setting, Euclidean prediction-centric interventions applied to the same *identical* final token were effective despite altering both norm and direction. Because the readout is taken from a fixed token whose angular alignment with prediction-relevant structure is preserved, simultaneous changes in norm and direction do not disrupt the underlying predictive geometry. The present analysis generalizes this observation by showing that, across non-identical tokens, predictive similarity in the prediction-centric phase is primarily indexed by angular organization rather than by overall Euclidean proximity. Results for shuffled sequences show no consistent angular–prediction alignment, serving as a negative control and indicating that the observed effects depend on structured context rather than token identity alone.

Together, these findings support a bi-phasic computational organization and point to a two-component geometric coding scheme in the prediction-centric phase: angular organization functions as a global signal aligned with prediction distributions across tokens, while representation norms encode token- and context-specific information that does not

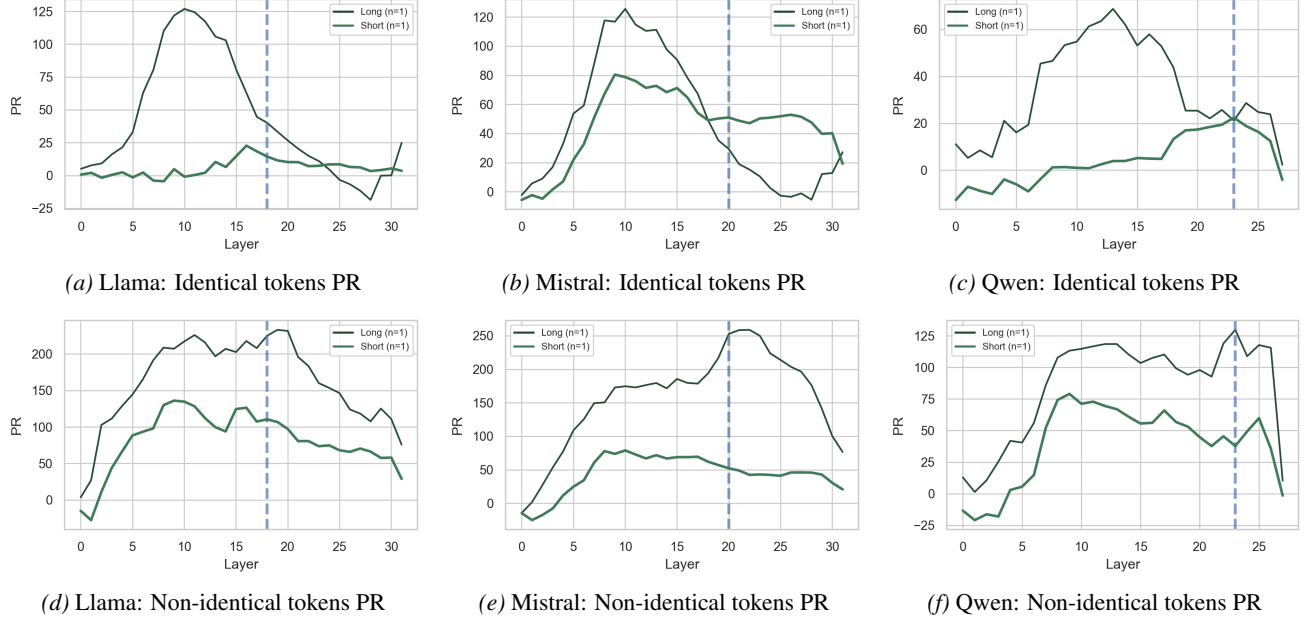


Figure 2. Per-layer participation ratio (PR) of normalized pilot-token representations for ordered long and short sequences, with shuffled counterparts shown as baselines. **Top row:** identical tokens. **Bottom row:** non-identical tokens. Columns correspond to models (Llama, Mistral, Qwen, left to right). The blue vertical line marks the perturbation-based phase-change point.

directly track predictive similarity. This leads to a testable hypothesis: interventions that selectively modify angular structure should be effective in the prediction-centric phase, but not in the input-centric phase. We next test this prediction.

**Angular interventions selectively affect the prediction-centric phase.** Previous results suggest that angular organization in the second computational phase carries prediction-aligned information. This leads to the hypothesis that angular interventions should be effective in the prediction-centric phase of the model, but not in the input-centric phase. We test this hypothesis using a purely angular intervention on the Months task.

Unlike the previous interventions, we design a new, purely directional intervention. Prior to computing centroids, we normalize all representation vectors, so that centroid vectors become average direction vectors, thus avoiding leaking norm information. For each token representation we intervene on (whether input- or prediction-based), we then normalize the token vector, replace its direction with that of the desired centroid direction, and finally rescale it to its original norm. This procedure alters only the representation’s direction while preserving its original magnitude.

In line with our predictions, input-based angular interventions fail across all layers of the model, whereas output-based angular interventions remain potent in the second, prediction-centric phase (Fig. 4). To further stress this dissociation, we additionally perform a purely norm-based

intervention, in which token representations are rescaled to match the mean norm of the corresponding centroid vectors. This intervention fails across all layers and all intervention types (Fig. 4).

One possible explanation for this dissociation follows directly from the structure of the final readout. Ignoring bias terms for simplicity, the output distribution for a token representation  $h_L$  at the final layer can be written as:  $p(\text{output tokens}) = \text{Softmax}(W_{\text{out}}h_L)$ , where  $W_{\text{out}}$  is the un-embedding matrix. Changing notation to separate norm and direction we can write:  $p(\text{output tokens}) = \text{Softmax}(W_{\text{out}}\|h_L\|_2\hat{h}_L)$ . This decomposition makes explicit that the direction of  $h_L$  determines the relative logit values across vocabulary entries, while the norm of  $h_L$  acts as a global scaling factor analogous to an inverse temperature, modulating the sharpness of the output distribution. This structure provides a mechanistic rationale for why selectively modifying angular structure is sufficient to alter prediction identity in the prediction-centric phase.

## 4. Conclusion

A central contribution of this work is to clarify the relationship between two prominent but often disconnected approaches to analyzing large language models. Specifically, geometric analyses of internal representational dynamics (Ethayarajh, 2019; Barbero et al., 2024; Cheng et al., 2025; Skean et al., 2025; Sarfati et al., 2024; Hosseini & Fedorenko, 2023; Skean et al., 2025; Cai et al., 2021; Raz-

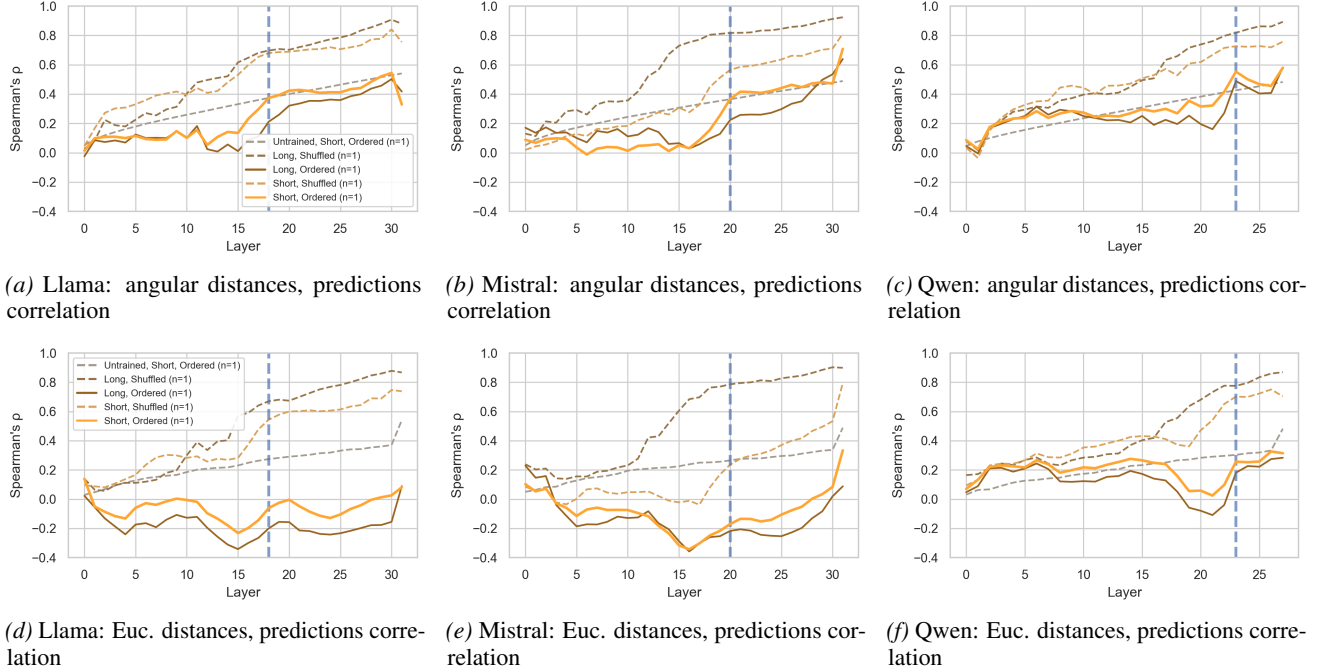


**Figure 3.** Per-layer correlation between non-identical tokens’ pairwise distances and pairwise prediction-distribution symmetric KL divergence, shown across layers. **Top row:** angular distances. **Bottom row:** Euclidean distances. Rows correspond to distance metrics, and columns correspond to models. The blue vertical line marks the perturbation-based phase-change point.

zhigaev et al., 2024) and intervention-based, output-oriented analyses of mechanism Turner et al., 2023; Engels et al., 2025; Yu et al., 2025. Our results suggest a reconciliation between these perspectives. Geometric analyses recover structured organization in latent space, however only part of this structure is causally operative in determining prediction. In particular, while both early and late layers exhibit rich and decodable geometric structure, only late-layer angular organization supports selective causal control over prediction identity. From this perspective, geometry, while descriptively relevant across all layers, becomes mechanistically relevant only in later-layers when it is aligned with the computation that directly forms the output distribution.

An open question raised by our findings concerns the architectural and optimization biases that may favor angular, rather than norm-based, coding in prediction-forming layers. Modern transformer architectures make extensive use of normalization schemes such as RMSNorm, which explicitly normalize or constrain representation magnitudes while preserving directional information (Zhang & Sennrich, 2019). While normalization alone does not imply angular coding, it plausibly creates favorable conditions under which direction becomes a more reliable and functionally meaningful signal than magnitude. More generally, understanding how network architecture design principles, such as normalization, self-attention, and residual connections interact to promote angularly organized prediction geometry remains an impor-

tant direction for future work (He et al., 2016; Vaswani et al., 2017; Zhang & Sennrich, 2019). From this perspective, angular coding may emerge as a byproduct of architectural choices that stabilize optimization while compressing norm-based degrees of freedom.

Our results also connect naturally to the widespread use of angular distance (e.g., cosine similarity) as a measure of semantic similarity (Mikolov et al., 2013) and as a characteristic feature of representational geometry (Hosseini & Fedorenko, 2023). Angular similarity has long been observed to correlate with semantic relatedness in word embeddings and contextual representations, yet the functional role of this geometry in decoder-based LLMs has remained ambiguous. Our findings provide a mechanistic grounding for this practice in late layers of decoder-only LLMs: angular proximity does not merely reflect semantic similarity but parametrizes similarity between output prediction distributions. At the same time, our results caution against interpreting angular similarity uniformly across depth, as early-layer angular structure, while present and decodable, does not support causal manipulation of prediction.

These distinctions have direct implications for understanding and control of large language models (Gilpin et al., 2018; Pan et al., 2025). Much prior work implicitly assumes that decodable or separable structure, whether semantic, behavioral, or safety-related (Saglam et al., 2025), constitutes a suitable target for intervention. Our results highlight a

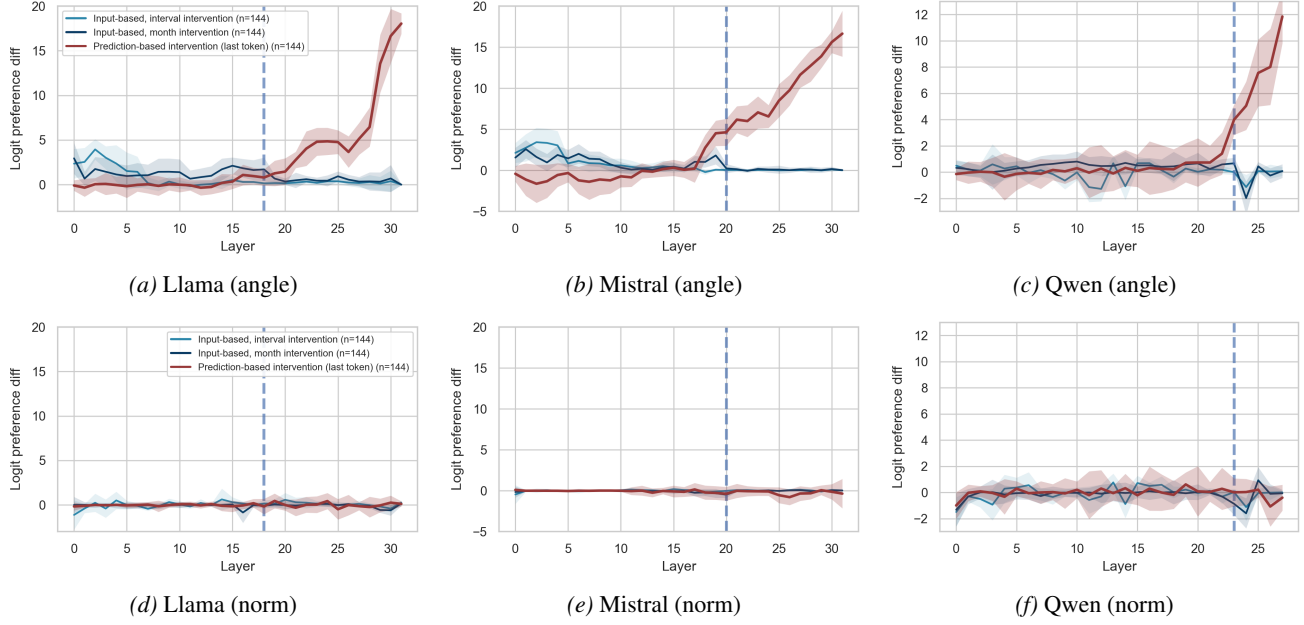


Figure 4. Per-layer intervention experiment results. **Top row:** pure angular interventions. **Bottom row:** pure norm interventions. Average logit preference difference is shown: blue curves correspond to input-based interventions (interval and month), red curves to output-based interventions. The blue vertical line marks the original perturbation-based phase-change point.

limitation of this assumption: decodable representational structure may be geometrically redundant with respect to the mechanisms that actually govern prediction. As a result, interventions that target easily decodable features may fail to generalize or may exert only indirect control (Ravichander et al., 2021; Hewitt & Liang, 2019; Elazar et al., 2020). By contrast, interventions aligned with causally meaningful geometric degrees of freedom, such as late-layer angular structure, offer a more principled basis for reliable control e.g. geometry-aware, layer-specific adapters (Hu et al., 2021). Furthermore, our results suggest that evaluating intervention strategies should involve not only detectability or linear separability, but the characterization of mechanistically-relevant geometry.

### Limitations and Future Work

This work has several limitations. First, our analysis focuses on a single class of tasks and model architectures, and it remains unclear how broadly the identified geometric schema generalizes across tasks, modalities, or training regimes. Second, while we identify a sharp transition from context-processing to prediction-forming computation, the relationship between early-layer context geometry (e.g. dimensionality expansion) and the emergence of prediction-aligned angular codes is not yet understood. One possibility is that early layers prepare a high-dimensional contextual basis from which late layers select and stabilize angularly organized predictive directions, but this hypothesis remains speculative. Finally, our analysis emphasizes representa-

tions averaged across contexts and does not address the context-dependent dynamics by which token representations are transformed during multi-step or algorithmic tasks, where intermediate state evolution may play a dominant role.

### Impact Statement

The work is foundational in nature and does not propose new deployment, safety, or policy interventions; its primary impact is to improve scientific understanding of how large language models compute predictions. Our findings may inform future approaches to model interpretation, fine-tuning, and control by highlighting the importance of targeting causally operative internal structure.

### References

Adebayo, J., Gilmer, J., Muelly, M., Goodfellow, I., Hardt, M., and Kim, B. Sanity checks for saliency maps. In Bengio, S., Wallach, H., Larochelle, H., Grauman, K., Cesa-Bianchi, N., and Garnett, R. (eds.), *Advances in Neural Information Processing Systems 31 (NeurIPS 2018)*. Curran Associates, Inc., 2018. URL [https://proceedings.neurips.cc/paper\\_files/paper/2018/hash/294a8ed24b1ad22ec2e7efea049b8737-Abstract.html](https://proceedings.neurips.cc/paper_files/paper/2018/hash/294a8ed24b1ad22ec2e7efea049b8737-Abstract.html).

Alain, G. and Bengio, Y. Understanding intermediate

layers using linear classifier probes. *arXiv preprint arXiv:1610.01644*, 2016.

Barbero, F., Banino, A., Kapturowski, S., Kumaran, D., Araújo, J. G. M., Vitvitskyi, A., Pascanu, R., and Veličković, P. Transformers need glasses! information over-squashing in language tasks. In *Advances in Neural Information Processing Systems (NeurIPS 37)*. arXiv, 2024. doi: 10.48550/arXiv.2406.04267. URL <https://arxiv.org/abs/2406.04267>.

Cai, X., Huang, J., Bian, Y., and Church, K. Isotropy in the contextual embedding space: Clusters and manifolds. *arXiv preprint arXiv:2109.05443*, 2021.

Cheng, E., Doimo, D., Kervadec, C., Macocco, I., Yu, J., Laio, A., and Baroni, M. Emergence of a high-dimensional abstraction phase in language transformers, April 2025. URL <http://arxiv.org/abs/2405.15471>. arXiv:2405.15471 [cs].

Conneau, A., Kruszewski, G., Lample, G., Barrault, L., and Baroni, M. What you can cram into a single vector: Probing sentence embeddings for linguistic properties. *arXiv preprint*, arXiv:1805.01070, 2018. URL <https://arxiv.org/abs/1805.01070>.

Dubey, A., Jauhri, A., Pandey, A., Kadian, A., Al-Dahle, A., Letman, A., Mathur, A., Schelten, A., Vaughan, A., Yang, A., Fan, A., Goyal, A., Hartshorn, A., Yang, A., ..., and many others. The llama 3 herd of models, 2024. URL <https://arxiv.org/abs/2407.21783>. arXiv:2407.21783 [cs.AI].

Elazar, Y., Ravfogel, S., Jacovi, A., and Goldberg, Y. Amnesic probing: Behavioral explanation with amnesic counterfactuals. *arXiv preprint*, arXiv:2006.00995, 2020. URL <https://arxiv.org/abs/2006.00995>.

Engels, J., Michaud, E. J., Liao, I., Gurnee, W., and Tegmark, M. Not all language model features are one-dimensionally linear, February 2025. URL <http://arxiv.org/abs/2405.14860>. arXiv:2405.14860 [cs].

Ethayarajh, K. How contextual are contextualized word representations? comparing the geometry of bert, elmo, and gpt-2 embeddings. *arXiv preprint arXiv:1909.00512*, 2019. URL <https://arxiv.org/abs/1909.00512>.

Gilpin, L. H., Bau, D., Yuan, B. Z., Bajwa, A., Specter, M., and Kagal, L. Explaining explanations: An overview of interpretability of machine learning. *arXiv preprint*, arXiv:1806.00069, 2018. URL <https://arxiv.org/abs/1806.00069>.

He, K., Zhang, X., Ren, S., and Sun, J. Deep residual learning for image recognition. In *Proceedings of the IEEE Conference on Computer Vision and Pattern Recognition (CVPR)*, pp. 770–778, 2016. URL [https://openaccess.thecvf.com/content\\_cvpr\\_2016/html/He\\_Deep\\_Residual\\_Learning\\_CVPR\\_2016\\_paper.html](https://openaccess.thecvf.com/content_cvpr_2016/html/He_Deep_Residual_Learning_CVPR_2016_paper.html).

Hewitt, J. and Liang, P. Designing and interpreting probes with control tasks. In *Proceedings of the 2019 Conference on Empirical Methods in Natural Language Processing and the 9th International Joint Conference on Natural Language Processing (EMNLP-IJCNLP)*, pp. 2733–2743, Hong Kong, China, 2019. Association for Computational Linguistics. doi: 10.18653/v1/D19-1275. URL <https://aclanthology.org/D19-1275/>.

Hosseini, E. A. and Fedorenko, E. Large language models implicitly learn to straighten neural sentence trajectories to construct a predictive representation of natural language, 2023. URL <https://arxiv.org/abs/2311.04930>. arXiv:2311.04930 [cs.CL].

Hu, E. J., Shen, Y., Wallis, P., Allen-Zhu, Z., Li, Y., Wang, S., and Chen, W. Lora: Low-rank adaptation of large language models. *arXiv preprint*, arXiv:2106.09685, 2021. URL <https://arxiv.org/abs/2106.09685>.

Jain, S. and Wallace, B. C. Attention is not explanation. *arXiv preprint*, arXiv:1902.10186, 2019. URL <https://arxiv.org/abs/1902.10186>. Accepted as NAACL 2019 Long Paper.

Jiang, A. Q., Sablayrolles, A., Mensch, A., Bamford, C., Chaplot, D. S., de las Casas, D., Bressand, F., Lengyel, G., Lample, G., Saulnier, L., Lavaud, L. R., Lachaux, M.-A., Stock, P., Le Scao, T., Lavril, T., Wang, T., Lacroix, T., and El Sayed, W. Mistral 7b, 2023. URL <https://arxiv.org/abs/2310.06825>. arXiv:2310.06825 [cs.CL].

Lad, V., Lee, J. H., Gurnee, W., and Tegmark, M. The remarkable robustness of llms: Stages of inference?, June 2025. URL <https://arxiv.org/abs/2406.19384>. arXiv:2406.19384 [cs].

Lapuschkin, S., Wäldchen, S., Binder, A., Montavon, G., Samek, W., and Müller, K.-R. Unmasking clever hans predictors and assessing what machines really learn. *Nature Communications*, 10(1):1096, 2019. doi: 10.1038/s41467-019-08987-4. URL <https://www.nature.com/articles/s41467-019-08987-4>.

Merity, S., Xiong, C., Bradbury, J., and Socher, R. Pointer sentinel mixture models. In *International Conference on Learning Representations*, 2017. URL <https://arxiv.org/abs/1609.07843>.

Mikolov, T., Yih, W.-t., and Zweig, G. Linguistic regularities in continuous space word representations. In *Proceedings of the 2013 Conference of the North American Chapter of the Association for Computational Linguistics: Human Language Technologies*, pp. 746–751, Atlanta, Georgia, 2013. Association for Computational Linguistics. URL <https://aclanthology.org/N13-1090/>.

Pan, B., Li, Y., Zhang, W., Lu, W., Xu, M., Zhou, S., Zhu, Y., Zhong, M., and Qian, T. A survey on training-free alignment of large language models. In *Findings of the Association for Computational Linguistics: EMNLP 2025*, pp. 4445–4461. Association for Computational Linguistics, 2025. doi: 10.18653/v1/2025.findings-emnlp.238. URL <https://aclanthology.org/2025.findings-emnlp.238/>.

Park, K., Choe, Y. J., and Veitch, V. The linear representation hypothesis and the geometry of large language models. *arXiv preprint*, arXiv:2311.03658, 2023. doi: 10.48550/arXiv.2311.03658. URL <https://arxiv.org/abs/2311.03658>.

Qwen, Yang, A., Yang, B., Zhang, B., Hui, B., Zheng, B., Yu, B., Li, C., Liu, D., Huang, F., Wei, H., Lin, H., Yang, J., Tu, J., Zhang, J., Yang, J., Yang, J., Zhou, J., Lin, J., Dang, K., Lu, K., Bao, K., Yang, K., Yu, L., Li, M., Xue, M., Zhang, P., Zhu, Q., Men, R., Lin, R., Li, T., Tang, T., Xia, T., Ren, X., Ren, X., Fan, Y., Su, Y., Zhang, Y., Wan, Y., Liu, Y., Cui, Z., Zhang, Z., and Qiu, Z. Qwen2.5 technical report, 2025. URL <https://arxiv.org/abs/2412.15115>. arXiv:2412.15115 [cs.CL].

Ravichander, A., Belinkov, Y., and Hovy, E. Probing the probing paradigm: Does probing accuracy entail task relevance? In *Proceedings of the 16th Conference of the European Chapter of the Association for Computational Linguistics: Main Volume*, pp. 3363–3377, Online, 2021. Association for Computational Linguistics. doi: 10.18653/v1/2021.eacl-main.295. URL <https://aclanthology.org/2021.eacl-main.295/>.

Razzhigaev, A., Mikhalchuk, M., Goncharova, E., Oseledets, I., Dimitrov, D., and Kuznetsov, A. The shape of learning: Anisotropy and intrinsic dimensions in transformer-based models, February 2024. URL <https://arxiv.org/abs/2311.05928>. arXiv:2311.05928 [cs].

Ribeiro, M. T., Singh, S., and Guestrin, C. “why should i trust you?”: Explaining the predictions of any classifier. pp. 97–101, 2016. doi: 10.18653/v1/N16-3020. URL <https://aclanthology.org/N16-3020/>.

Saglam, B., Kassianik, P., Nelson, B., Weerawardhena, S., Singer, Y., and Karbasi, A. Large language models encode semantics in low-dimensional linear subspaces, August 2025. URL <http://arxiv.org/abs/2507.09709>. arXiv:2507.09709 [cs].

Sarfati, R., Liu, T. J. B., Boullé, N., and Earls, C. J. Lines of thought in large language models, 2024. URL <https://arxiv.org/abs/2410.01545>. arXiv:2410.01545 [cs].

Skean, O., Arefin, M. R., Zhao, D., Patel, N., Naghiyev, J., LeCun, Y., and Shwartz-Ziv, R. Layer by layer: Uncovering hidden representations in language models, jun 2025. URL <http://arxiv.org/abs/2502.02013>. arXiv:2502.02013 [cs].

Turner, A. M., Thiergart, L., Leech, G., Udell, D., Vazquez, J. J., Mini, U., and MacDiarmid, M. Steering language models with activation engineering, 2023. URL <https://arxiv.org/abs/2308.10248>. arXiv:2308.10248 [cs.CL].

Vaswani, A., Shazeer, N., Parmar, N., Uszkoreit, J., Jones, L., Gomez, A. N., Kaiser, Ł., and Polosukhin, I. Attention is all you need. In Guyon, I., Luxburg, U. V., Bengio, S., Wallach, H., Fergus, R., Vishwanathan, S., and Garnett, R. (eds.), *Advances in Neural Information Processing Systems 30*, pp. 5998–6008, 2017. URL <https://proceedings.neurips.cc/paper/2017/file/3f5ee243547dee91fb053c1c4a845aa-Paper.pdf>.

Yu, S., Bulusu, V., Yasunaga, O., Lau, C., Blondin, C., O’Brien, S., Zhu, K., and Sharma, V. From directions to cones: Exploring multidimensional representations of propositional facts in llms, May 2025. URL <http://arxiv.org/abs/2505.21800>. arXiv:2505.21800 [cs].

Zhang, B. and Sennrich, R. Root mean square layer normalization. *arXiv preprint*, arXiv:1910.07467, 2019. URL <https://arxiv.org/abs/1910.07467>.

## S1. Supplementary Material

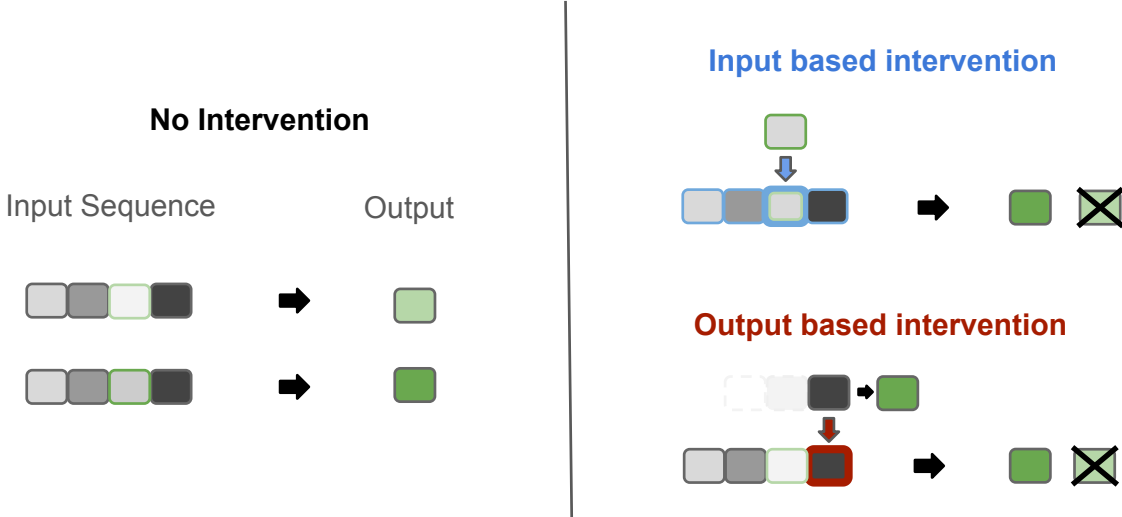


Figure S1. Visual illustration of two intervention strategies. Each square denotes a token representation. Input-based intervention (blue) perturbs the representation of a selected input token using the representation of another token, effectively modifying the input sequence prior to generation. Output-based intervention (red) directly manipulates the representation of the final token to steer the model’s output toward a desired target, using alternative representations known to produce that output.

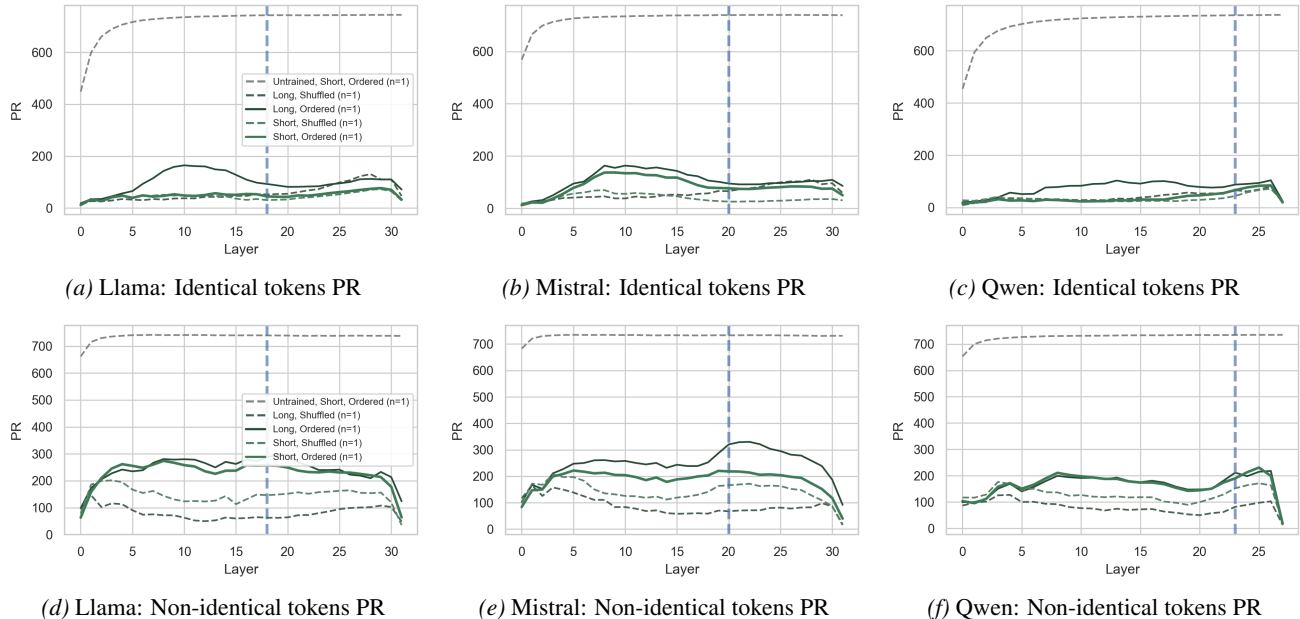


Figure S2. Per-layer participation ratio (PR) for normalized token representations. Columns correspond to models (left to right: Llama, Mistral, Qwen). Blue vertical line corresponds to phase change point based on perturbations. Top row shows identical tokens and bottom row shows non-identical tokens.

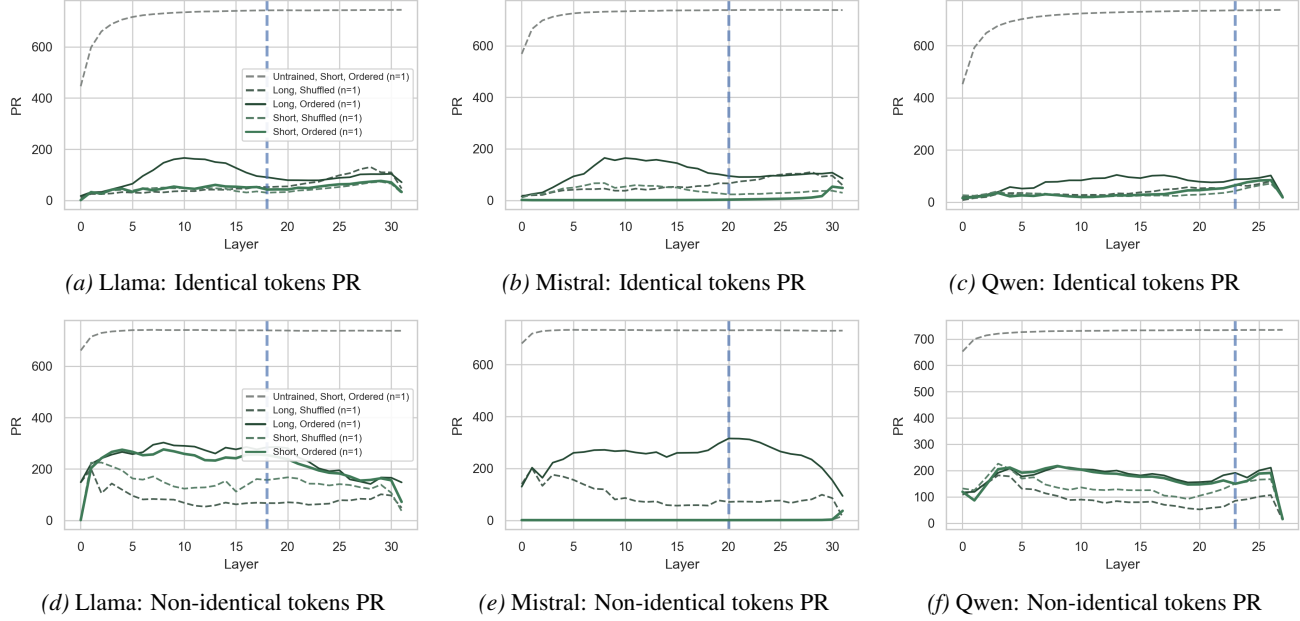


Figure S3. Per-layer participation ratio (PR) for token representations. Rows correspond to models. Columns are different token sets. The blue vertical line marks the perturbation-based phase-change point.

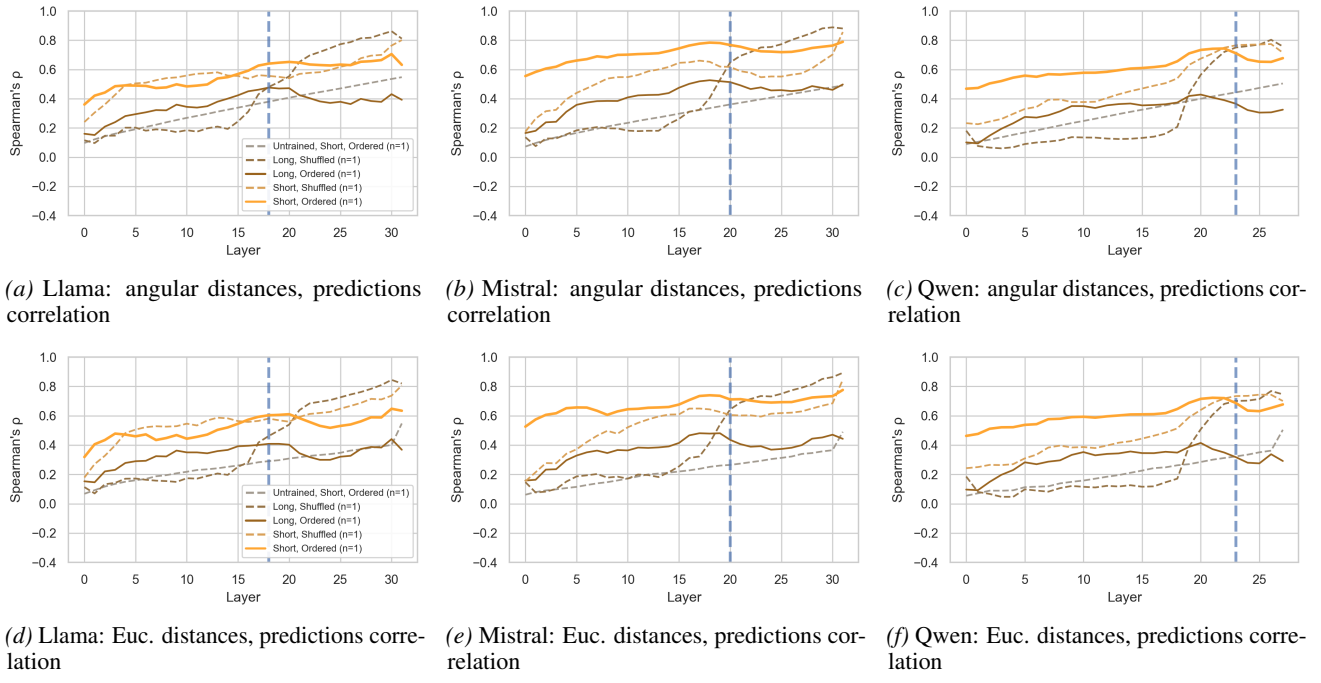


Figure S4. Per-layer correlation between identical tokens' pairwise distances and pairwise prediction-distribution symmetric KL divergence. The blue vertical line marks the perturbation-based phase-change point. Rows correspond to models, columns are distance metrics.